

AEDC-TR-73-143

cy 2

OCT 11 1973  
NOV 7 1973

JUN 10 1986  
MAY 5 1994



# A STUDY OF ELECTRODELESS ARC DISCHARGE USING ARGON, NITROGEN, AND AIR

Dennis R. Keefer  
University of Florida

September 1973

Approved for public release; distribution unlimited.

ENGINEERING REPORTS  
FILE COPY

**ARNOLD ENGINEERING DEVELOPMENT CENTER  
AIR FORCE SYSTEMS COMMAND  
ARNOLD AIR FORCE STATION, TENNESSEE**

PROPERTY OF U.S. AIR FORCE  
AEDC TECHNICAL LIBRARY

Property of U. S. Air Force  
AEDC LIBRARY  
NOV 7 1973

# ***NOTICES***

When U. S. Government drawings specifications, or other data are used for any purpose other than a definitely related Government procurement operation, the Government thereby incurs no responsibility nor any obligation whatsoever, and the fact that the Government may have formulated, furnished, or in any way supplied the said drawings, specifications, or other data, is not to be regarded by implication or otherwise, or in any manner licensing the holder or any other person or corporation, or conveying any rights or permission to manufacture, use, or sell any patented invention that may in any way be related thereto.

Qualified users may obtain copies of this report from the Defense Documentation Center.

References to named commercial products in this report are not to be considered in any sense as an endorsement of the product by the United States Air Force or the Government.

**A STUDY OF ELECTRODELESS ARC DISCHARGE  
USING ARGON, NITROGEN, AND AIR**

**Dennis R. Keefer  
University of Florida**

**Approved for public release; distribution unlimited.**

## FOREWORD

The work reported herein was sponsored by the Arnold Engineering Development Center (AEDC), Air Force Systems Command (AFSC), Arnold Air Force Station, Tennessee, under Program Element 65802F.

The results of research were obtained by the Aerospace Engineering Department, University of Florida, during the period from January 1972 to March 1973, under Contract F40600-72-C-0005. The report was submitted July 31, 1973, for publication.

The author gratefully acknowledges the contributions of graduate students John Saxton and Gary Harloff to the research effort and Mr. John Allen for the preparation of the figures.

The reproducibles used in the reproduction of this report were supplied by the author.

This technical report has been reviewed and is approved.

MAURICE A. CLERMONT  
Major, CF  
Research and Development Division  
Directorate of Technology

ROBERT O. DIETZ  
Director of Technology

**ABSTRACT**

A study of the bluff-body stabilized electrodeless arc was undertaken to extend the operation to greater mass flow rates and power input. A small arc chamber, operating at a frequency of 3.5 MHz, was operated with mass flows up to 1.026 gm/sec of argon at atmospheric pressure with a power input of 6.79 KW. Under these conditions a plasma bulk temperature of 2305°K was obtained with a heating efficiency of 18%. It was found that heating efficiency increased with chamber pressure, but bulk temperature depends primarily upon the power input. A larger arc chamber was designed for a nominal power input of 200 KW at a frequency of 377 MHz. This chamber was operated at mass flow rates up to 2.4 gm/sec of argon at a pressure of two atmospheres. A plasma bulk temperature of 5856°K was obtained at a power input of 76 KW. Attempted operation using air as a working fluid was unsuccessful at pressures in excess of 2/3 atmosphere due to inefficient coupling to the arc plasma.

## TABLE OF CONTENTS

ABSTRACT .....	iii
LIST OF ILLUSTRATIONS .....	v
NOMENCLATURE .....	vii
I. INTRODUCTION .....	1
II. THEORETICAL INVESTIGATION .....	2
III. EXPERIMENTAL STUDY OF A LOW POWER BLUFF-BODY STABILIZED ELECTRODELESS ARC .....	4
IV. DESIGN ANALYSIS OF THE LARGE ARC CHAMBER .....	6
V. EXPERIMENTS WITH THE LARGE ARC CHAMBER .....	11
VI. OPERATION OF ELECTRODELESS ARCS IN AIR .....	14
VII. SUMMARY .....	16
REFERENCES .....	17

## TABLES

1. Small Arc Data - Reamed Orifices.....	19
2. Small Arc Data - Laval Shaped Orifice .....	20

## ILLUSTRATIONS

Figure

1. Model for boundary layer analysis showing velocity boundary layers, $\delta$ , and thermal boundary layers $\beta$ .....	22
2. Simplified boundary layer model for incompressible flow without heat addition .....	23
3. Calculated boundary layer profiles for a Reynolds number of 300 .....	24

Figure

4.	Axial velocity profiles at three axial locations. Reynolds number = 300, $U_o/u_o = 4$ .....	25
5.	Radial velocity profiles at three axial locations. Reynolds number = 300, $U_o/u_o = 4$ .....	26
6.	Remote tuned circuit used in the 4.5 MHz experiments.....	27
7.	Heating efficiency of the 4.5 MHz arc at three values of pressure.....	28
8.	Enthalpy for the 4.5 MHz arc at three values of pressure.....	29
9.	Temperatures used in the design analysis.....	30
10.	Heat transfer rate as a function of annulus width.....	31
11.	Upper portion of the large arc chamber.....	32
12.	Lower portion of the large arc chamber.....	33
13.	Bulk temperatures in three electrodeless arcs. Open circles are for 4.5 MHz vortex stabilized arc, closed circles are for 4.5 MHz bluff-body stabilized arc and squares are for 3.77 MHz bluff-body stabilized arc.....	34
14.	Electrical conductivity of argon and air at one atmosphere.....	35
15.	Thermal conductivity of argon and air at one atmosphere.....	36
16.	Possible temperature profile resulting from increase in thermal conductivity associated with molecular dissociation of air.....	37

## Nomenclature

$a$	Radius
$A^*$	Cross-sectional area
$c$	Attachment coefficient
$C_d$	Discharge coefficient
$C_p$	Heat capacity at constant pressure
$d$	Bolt circle diameter
$D_o$	Quartz tube inner diameter
$D_l$	Quartz tube outer diameter
$E$	Young's modulus
$F_{tu}$	Ultimate tensile stress
$h_l$	Liquid film coefficient
$k$	Quartz thermal conductivity
$l$	Tube length
$L$	Tube radius
$\dot{m}$	Mass flow rate
$P_o$	Chamber pressure
$P_w$	Wall pressure
$q$	Heat transfer rate
$Q$	Heat flux per unit length
$r$	Radial coordinate
$R$	(pp. 7) Gas constant
$R$	(pp. 13) Tube mean radius
$R_2$	Acrylic tube inner radius
$R_3$	Acrylic tube outer radius
$s_1$	Axial thermal stress
$s_2$	Tangential thermal stress
$t$	Quartz tube thickness
$t_c$	Head cover thickness
$T_{L-enter}$	Entering water temperature
$T_{L-exit}$	Exiting water temperature
$T_o$	Upstream stagnation temperature

$T_{q \&}$	Outer quartz wall temperature
$T_{wq}$	Inner quartz wall temperature
$u_o$	Inner flow velocity
$U$	Overall heat transfer coefficient
$U_o$	Outer flow velocity
$v_r$	Radial velocity
$v_z$	Axial velocity
$v_{za}$	Point of flow reversal
$v_{zc}$	Maximum axial velocity
$Z$	Axial coordinate
$\alpha$	Thermal expansion coefficient
$\beta_I$	Inner thermal boundary layer
$\beta_{III}$	Outer thermal boundary layer
$\gamma$	Ratio of specific heats
$\delta$	Skin depth
$\delta_I$	Inner velocity boundary layer
$\delta_{II}$	Outer velocity boundary layer
$\Delta P$	Pressure difference
$\lambda$	Thermal conductivity
$\mu$	Permeability
$\nu$	Poisson's ratio
$\sigma$	Electrical conductivity
$\omega$	Angular frequency

## SECTION I

### INTRODUCTION

Electrodeless discharges have long been used as sources of laboratory plasmas, but recently it has been proposed to use high pressure, high power electrodeless arcs as a source of high enthalpy gases. The electrodeless arc would eliminate the contamination of the hot gas caused by the erosion of electrodes in a conventional D.C. arc, and may provide a means of reducing the radiation losses.

The first successful operation of the electrodeless discharge as an arc at atmospheric pressure was obtained by Reed (Ref. 1) who found that the arc could be stabilized by means of a small vortex flow in a confining cylindrical tube. This means of stabilization works well at small flow rates, but when the flow is increased the arc becomes unsteady and eventually blows out. It was found that this problem could be overcome by the use of a bluff-body in the flow to generate a vortex ring in the arc region (Ref. 2). It was also found that the bluff-body enhanced the transfer of energy from the hot plasma to the flowing gas, producing higher exhaust temperatures.

The present study was undertaken to extend the measurements to higher values of mass flow and power input and attempt to obtain successful operation of the bluff-body stabilized arc in air. In addition, a modest effort was made to extend the boundary layer analysis of Martin and Keefer (Ref. 3) to the case of an axisymmetric confined arc.

Section II contains a description of the theoretical analysis using a boundary layer technique. Experiments which extended the operation of the arc to higher mass flow rates and input power are described in Section III. Section IV presents a detailed design analysis for a larger arc chamber and Section V describes experiments using this chamber. A discussion of the problems involved in the operation of an electrodeless arc in air is contained in Section VI, and a summary is presented in Section VII.

## SECTION II

## THEORETICAL INVESTIGATION

A modest attempt was made to extend the analysis of Martin and Keefer (Ref. 3) to the case of an axisymmetric flow representative of the conditions downstream of the bluff-body. Downstream of the bluff-body, a cool annular flow of relatively high velocity mixes with an inner cylindrical flow of higher temperature and lower velocity. The flow in this region generates a vortex with correspondingly large radial velocity components and recirculating flow. A complete solution for the flow field in this region would entail a solution to the two-dimensional equations of fluid mechanics with heat addition.

An analysis of this type is exceedingly complex and is beyond the scope of this study. Therefore, an attempt was made to describe the flow using an integral boundary layer approach. An assumption that radial velocity components are small is inherent in this technique, and it was realized that the solution would only apply in the region immediately downstream of the bluff-body where the radial velocity is small.

The model chosen for analysis is shown in Figure 1. The inner velocity boundary layer,  $\delta_I$ , extends from the axis to the point where flow reversal occurs,  $v_{za}$ , and the outer velocity boundary layer,  $\delta_{II}$ , extends to the velocity maximum,  $v_{zc}$ . The inner thermal boundary layer,  $\beta_I$ , extends from the axis to a point where the temperature is a maximum and the outer boundary layer,  $\beta_{III}$ , is arbitrarily taken as one-half the initial maximum temperature assigned a priori at the edge of the bluff body. The problem becomes one of finding the boundary layer thicknesses as a function of the axial coordinate for given initial conditions and energy input using arbitrarily determined velocity profiles.

To lend insight into the behavior of the flows described by this model, a simple calculation was performed for the case of an incompressible fluid with no heat addition, and with initially uniform flow velocities. The situation is shown in Figure 2. The inner flow has a velocity of  $u_o$  and the outer flow velocity is  $U_o$ . The radial distance over which the inner flow is uniform is  $\delta_I$  and the radial distance at which the flow reaches the outer flow velocity,  $U_o$ , is  $\delta_I + \delta_{II}$ .

Radial and axial coordinates are made dimensionless by dividing by the tube radius,  $L$ . The problem consists of determining the boundary layer thicknesses  $\delta_I$  and  $\delta_{II}$  together with the wall pressure,  $P_w$ , as a function of the axial coordinate. The velocity inside the mixing layer is assumed to have the form

$$v_z = U_o - \left( \frac{U_o - u_o}{2} \right) \left\{ 1 + \cos \pi \left[ \frac{r - \delta_I}{\delta_{II}} \right] \right\} \quad (1)$$

This form is chosen following Peters (Ref. 4), because it is continuous and matches the inner and outer velocities. Integration of the continuity equation and the axial boundary layer equation with respect to the radial coordinate yields a set of coupled, ordinary equations in  $\delta_I$ ,  $\delta_{II}$  and  $P_w$ . The equations are derived in detail by Harloff (Ref. 5).

The system of ordinary equations was solved numerically for various ratios of outer to inner flow velocity,  $U_o/u_o$ , for a constant Reynolds number of 300 based on the outer flow velocity, in a tube where the initial mixing occurs at  $r/L = 0.5$ . The results are shown in Figure 3. It can be seen that the curvature of the boundary layer toward the axis is very slight, and that the boundary layer grows very rapidly for the higher velocity ratios. Profiles of axial and radial velocity are shown in Figures 4 and 5 for  $U_o/u_o = 4$ , at three axial locations. The axial velocity profiles have the expected characteristics, but the inward radial velocity is of considerable magnitude near the initial mixing region. This behavior is inconsistent with the assumptions used to obtain the original equations.

Based on these results it was concluded that the integral boundary layer analysis would not yield meaningful results for the mixing region in the wake of a bluff-body where recirculation is occurring. A successful analysis of this complex flow will necessitate the solution of the complete system of nonlinear partial differential equations describing fluid flows with heat addition. The extensive analysis required was considered to be beyond the scope of the present study.

## SECTION III

EXPERIMENTAL STUDY OF A LOW POWER BLUFF-BODY  
STABILIZED ELECTRODELESS ARC

It has been found that the efficiency of the electrodeless arc, when used as a gas heater, is greatly enhanced by the use of a bluff-body stabilizer (Ref. 2). The improvement is obtained as a result of stable operation at increased mass-flow rates and enhanced mixing between the cool outer flow and the hot plasma core. A series of experiments was performed using a chamber of 4-inch diameter and 12-inch length operated at a nominal frequency of 3.5 MHz, using argon as a working fluid. The primary parameter of interest in the studies was the bulk temperature attained for various conditions of flow and power input.

The arc chamber consisted of a Pyrex tube cooled by an external air flow which utilized a water-cooled copper stabilizer of 2-inches diameter. The input coil consisted of six turns of 3/8-inch diameter copper tubing with a coil length of 4.15 inches and a mean diameter of 7.63 inches. The coil was part of a remotely tuned resonant circuit designed to allow accurate determination of the power delivered to the arc chamber. The circuit is shown in Figure 6. During arc operation the phase meter was used to tune the circuit for unity power factor and the power was determined from the voltage and current in the coaxial feed line. The power dissipated by the circuit itself and through induction heating of the arc chamber was determined by calibration with no arc present.

The bulk temperature in the arc is defined as the stagnation temperature existing upstream of the exhaust orifice, and was determined by measuring the mass flow through the orifice and the pressure in the arc chamber. Sonic flow in the orifice was assured by exhausting into a 20-cfm vacuum pump downstream of the orifice. Under conditions of choked flow the upstream stagnation temperature is related to the pressure and mass flow by

$$T_o = \left( \frac{P_o A^*}{\dot{m}} \right)^2 \frac{\gamma}{R} \left( \frac{2}{\gamma+1} \right)^{\frac{\gamma+1}{\gamma-1}} C_d^2 \quad (2)$$

where  $P_o$  is the arc chamber pressure,  $A^*$  is the cross-sectional area of the throat,  $\dot{m}$  is the mass flow,  $\gamma$  is the ratio of specific heats,

$R$  is the gas constant and  $C_d$  is the discharge coefficient. The discharge coefficient was determined as a function of Reynolds number for each orifice used by calibration, using room temperature flow. An iterative procedure was used in the data reduction to obtain the appropriate discharge coefficient for the prevailing flow Reynolds number.

Data were obtained over a range of mass flow rates and power inputs by utilizing a series of exhaust orifices of different diameter. For a given orifice diameter, the power input was reduced as the mass flow was increased to maintain a constant chamber pressure. When the power was reduced to the point that the arc extinguished, a larger exit orifice was used to obtain a further increase in mass flow.

The data of Reference 2 were extended to higher mass-flow rates, using exhaust orifices of 0.125 and 0.188 inch diameter and a nominal chamber pressure of one atmosphere. The results are summarized in Table 1, where the heating efficiency is defined as the product of mass-flow rate and enthalpy increase divided by the net power input to the arc. The balance of the energy is lost in the form of plasma radiation and thermal conduction to the arc chamber. A maximum flow rate of 1.026 gm/sec was attained with a power input of 6.79 KW. This results in a bulk gas temperature of 2305°K and a heating efficiency of 18%.

In order to determine the effect of chamber pressure, over a limited range, a series of experiments was performed at nominal chamber pressures of 2/3, 1 and 1-1/3 atmospheres. For the series of experiments a laval type exit nozzle was used, whose discharge coefficient was less sensitive to flow Reynolds number. These results have been summarized in Table 2. The bulk temperature in these experiments was consistently higher than those obtained using the sharp-edged orifices. This is due to the fact that the discharge coefficient of the nozzle is reduced at elevated temperature by increased viscous losses in the long flow passage. For this reason, the temperatures listed in Table 2 are probably higher than actually existed during the experiment.

Despite the uncertainty in the absolute value of temperature, the variation of heating efficiency with pressure is apparent. As the pressure is increased, the heating efficiency increases as shown in Figure 7. However, the enthalpy is not a strong function of pressure but depends primarily on the input power as can be seen in Figure 8. The temperature has essentially the same behavior as the enthalpy since, in this temperature range,  $C_p$  is approximately constant for argon.

These experiments have shown that the arc is stable at higher flow rates, and that the heating efficiency can be expected to increase with increasing arc pressure. The gas temperature is not a strong function of pressure, but is essentially dependent on the power delivered to the plasma.

## SECTION IV

## DESIGN ANALYSIS OF THE LARGE ARC CHAMBER

The large arc chamber was designed to investigate bluff-body stabilization of the electrodeless arc at pressures up to ten atmospheres. The power was to be supplied by a 200 kw r-f generator, operating at 377 KHz, and high temperatures in the chamber were expected. For this reason, and because visual observations were important, the chamber was made from a quartz tube. The quartz tube was to be water cooled, so a clear acrylic tube was chosen to be the water jacket. The clear acrylic tube would also allow visual observation of the plasma. One of the major design concerns was to keep the quartz tube from carrying any loads except thermal loads. The water cooling system was, therefore, pressurized and the acrylic tube would take the pressure loads. The mechanical loads on the quartz tube, due to sealing, were reduced by specially designed seals. In order to minimize induction heating, the head covers were made from aluminum and attached with brass bolts.

The safety factors used were 1.5 to limit and then 2.5 to ultimate. This gave a total safety factor of 3.75. The system was designed to ultimate loads. The pressures used were an internal pressure of 150 psi and an external pressure of 15 psi.

The first consideration was the amount of heat that the quartz tube could transfer to the cooling water. Figure 9 gives the positions of the various temperatures. The following assumptions were made:  $T_{wq} = 1273^{\circ}\text{K}$  (the maximum temperature of the quartz before it starts to soften),  $T_{L\text{-exit}} - T_{L\text{-enter}} = 28^{\circ}\text{K}$  (the capacity of the heat exchanger), and  $T_{L\text{-enter}} = 319^{\circ}\text{K}$  (based on the temperature limits of the acrylic). Based on considerations for the plasma, the quartz tube dimensions were chosen as: inside diameter = 4.0 inches, wall thickness - .1575 inch, and length - 24.0 inches.

The heat transfer rate,  $q$ , was given by Stoever (Ref. 6) as

$$q = UA(\Delta T_{\ell m}) \quad (3)$$

where  $U$  is the overall heat transfer coefficient and  $\Delta T_{\ell m}$  is

$$\frac{(T_{wq} - T_{\ell\text{-enter}}) - (T_{wq} - T_{\ell\text{-exit}})}{2.3 \log_{10} \left[ \frac{T_{wq} - T_{\ell\text{-enter}}}{T_{wq} - T_{\ell\text{-exit}}} \right]} \quad (4)$$

When

$$\frac{T_{wq} - T_{\ell\text{-enter}}}{T_{wq} - T_{\ell\text{-exit}}} < 2, \quad (5)$$

then  $\Delta T_{\ell m}$  can be approximated by

$$\frac{(T_{wq} - T_{\ell\text{-enter}}) + (T_{wq} - T_{\ell\text{-exit}})}{2} . \quad (6)$$

The overall heat transfer coefficient for this case was found by solving

$$\frac{1}{U} = \frac{t}{K} + \frac{D_o}{h_{\ell} D_1} \quad (7)$$

where  $D_o$  is the inside diameter of the quartz tube,  $D_1$  is the outside diameter of the quartz tube,  $t$  is the thickness of the quartz tube,  $K$  is the thermal conductivity of the quartz, and  $h_{\ell}$  is the liquid film coefficient.

To find  $h_{\ell}$ , graphs from Stoever were used. These graphs are based on the velocity of the water, the temperature of the water, and a corrected diameter. The velocity of the water was determined from the volume flow rate of the water and the size of the annulus between the quartz and the acrylic. To size the acrylic tube it was necessary to know how the heat transfer rate varied with the width of the annulus. The heat transfer rate was calculated for different annulus dimensions and the results are shown in Figure 10. From the results it can be seen that the annulus size does not greatly affect the heat transfer rate. The size of the acrylic tube was, therefore, chosen on the basis of the standard sizes available. For an acrylic tube with an inside diameter of 4.625 inches, the annulus width was .155 inch and the total heat transfer rate was 60.3 KW. This was the maximum amount of heat that could be transferred across the quartz tube. From this value of the heat transfer rate, the maximum temperature difference across the quartz tube can be found from

$$q = \frac{k \ 2\pi \ \ell \ (T_{wq} - T_{q\ell})}{2.3 \log_{10} (D_1/D_o)} \quad (8)$$

where  $\ell$  is the length of the tube. If  $D_1/D_o < 2$ , then equation (8) can be approximated by

$$q = \frac{k \ \pi \ \ell \ D_o}{t} (T_{wq} - T_{q\ell}) . \quad (9)$$

The temperature difference was calculated to be  $900^{\circ}\text{K}$  and  $T_{q\ell}$  was  $373^{\circ}\text{K}$ .

With the temperature difference known, the axial and tangential thermal stresses  $s_1$  and  $s_2$  can be found from Roark (Ref. 7) as

$$s_1 = s_2 = \frac{\Delta T \alpha E}{2(1-\nu)} \quad (10)$$

where  $\alpha$  is the coefficient of thermal expansion,  $E$  is Young's modulus, and  $\nu$  is Poisson's ratio. This gave a margin of safety of 1.28, where the margin of safety is given by

$$\frac{\text{Maximum Allowable Stress}}{\text{Calculated Stress}} - 1.$$

According to Roark the thermal stresses can be 25 percent higher at the ends of the tubes, and the margin of safety would be .82 at the ends.

When the system is operating at vacuum pressure during ignition, the quartz is subjected to an external pressure of 15 psi. The axial and tangential stresses,  $s_1$  and  $s_2$ , are given by Roark for thin cylinders as

$$s_1 = \frac{\Delta PR}{2t} \quad (11)$$

and

$$s_2 = \frac{\Delta PR}{t} \quad (12)$$

where  $R$  is the mean radius of the tube,  $t$  is the wall thickness and  $\Delta P$  is the pressure difference. The stress  $s_1$  was zero because there were no axial loads on the quartz. The stress  $s_2$  acts in the opposite direction (compression) from the thermal loads (tension) and reduces the stress level. With a vacuum on the chamber the margin of safety is 3.71.

To determine the effect if the water pressure was suddenly lost, the stresses were calculated with the full internal pressure of 150 psi but with no safety factors. These stresses were added to the thermal stresses. The margin of safety was .23 but at the ends it was only .08.

The acrylic tube was sized to take the ultimate pressure loads. The axial stress,  $s_1$ , tangential stress,  $s_2$ , and radial stress,  $s_3$ , were found from Roark, for thick cylinders, by

$$s_1 = \Delta P \frac{R_2^2}{R_3^2 - R_2^2} \quad (13)$$

$$s_2 = \Delta P \frac{R_3^2 + R_2^2}{R_3^2 - R_2^2} \quad (14)$$

$$s_3 = \Delta P. \quad (15)$$

The pressure difference is  $\Delta P$ , and  $R_2$  and  $R_3$  are the inner and outer radius, respectively. For an acrylic tube with the dimensions: inside diameter 4.625 inches, outside diameter 5.625 inches, and wall

thickness of .5 inch, the margin of safety was .97.

The flanges on the acrylic tube were sized to contain the same amount of material that would be in an acrylic flat cover for the tube. For a flat head cover, the thickness,  $t_c$ , is found from Roark by

$$t_c = d \sqrt{\frac{c\Delta P}{F_{tu}}} \quad (16)$$

where  $d$  is the diameter of the bolt circle,  $c$  is an attachment coefficient,  $\Delta P$  is the pressure difference, and  $F_{tu}$  is the ultimate tensile stress. The thickness of the flange was calculated to be 1.64 inches, but to provide better attachment a flange thickness of 2.0 inches was used.

The thickness of the aluminum head covers was also found by equation 3.13, but since the thickness required was only .28 inch, the size of the head covers will be determined by other design factors.

Once the acrylic and quartz tubes had been sized, the rest of the system was designed. The system was designed for the gas to flow downward. It has been found that this design results in greater plasma stability. The system was to be designed with as much flexibility as possible. The bluff body can be raised, lowered, or changed, and the entrance and exit nozzles can be changed without disturbing the rest of the system.

The quartz seals were designed to eliminate seal stresses. They were made from RTV-60 silicone and molded in a special mold. The seals completely enclosed the ends of the quartz and then slipped into a groove in the head covers. The grooves were 3/4 inch deep and the quartz fitted 1/2 inch down into them. The rest of the space was occupied by the RTV. This design compressed the quartz from both sides so there was only a compression load across the quartz and no hoop stresses.

The upper portion was designed in three parts, see Figure 11, (1) the upper head cover, (2) the water plenum, and (3) the bluff-body holder. The head cover contained a seal groove for the quartz. There were also 36 holes for the water to pass through and into the water plenum. The holes were sized such that their total cross-sectional area was greater than that of the water pipes to minimize the pressure drop. The head cover was sealed to the acrylic tube with an o-ring. The cross-sectional area of the water plenum was also made larger than that of the water pipes. It filled around the bluff-body holder and was sealed to the upper head cover with a flat impregnated gasket. Not only did the bluff-body holder support the bluff body, but it also housed the static pressure tap and the entrance nozzle. The bluff-body supports also served as the water cooling passages for the bluff body. An o-ring was used to seal the bluff-body holder to the upper head cover.

The lower portion was designed in two parts, see Figure 12, (1) the lower head cover and (2) the water plenum. The lower head cover was like the upper one in that it had the seal groove and 36 holes for water passage, but it was hemispherical in shape. The hemispherical shape provided a smooth flow of the hot gas towards the exhaust nozzle. This helped to protect the lower head cover from the high temperatures. The exhaust nozzle threaded into the base of the hemisphere. Part of the water plenum was the other side of the hemisphere. This cooled the hemisphere and further protected it. The water plenum fitted around the exhaust nozzle and completely cooled the lower section. The water entered through four holes to ensure even cooling of the hemisphere. The plenum had the attachment points for the exhaust heat exchanger. The entire lower portion was sealed with o-rings.

## SECTION V

## EXPERIMENTS WITH THE LARGE ARC CHAMBER

The large, cooled arc chamber, described in the previous section, was used to extend the data for argon to higher power and pressure and to attempt operation using nitrogen and air. The power supply used in these experiments was a Westinghouse induction heater which has a nominal power output of 200 KW. The operating frequency of this generator was approximately 377 KHz, nearly a factor of ten lower than that used in the previous experiments. These experiments, therefore, provide information on scaling with frequency.

For the experiments using argon as the working fluid the arc was driven with a remote tuned circuit similar to the one used in the previous experiments. There was one significant difference, however. In the previous experiments the circuit could be tuned, by means of a variable capacitor, while under load. Due to the large component sizes required with the lower frequency, no variable capacitor was available and the circuit could not be tuned while the arc was in operation. The circuit was tuned before the generator was turned on by changing the length of the work coil. This adjustment had to be made by trial and error to obtain a unity power factor for the loaded condition.

Cooling for the arc chamber was provided by a closed circuit system utilizing a water-to-water heat exchanger. The entire cooling system could be pressurized to balance the chamber pressure, reducing the mechanical load on the quartz inner tube. Flow meters and temperature sensors were provided to determine the heat removed from the chamber during steady-state operation. The hot exhaust gases passed through an orifice into a heat exchanger to reduce the exhaust temperature. As before, a vacuum pump insured that the flow in the orifice was sonic.

At the lower frequency used in these experiments, the discharge did not self-ignite when the chamber was evacuated. A weak capacitive discharge would start, but was of insufficient intensity to ignite the inductive arc. To obtain arc initiation it was necessary to increase the intensity of the capacitive discharge by tapping the work coil voltage through a current limiting inductance. Using this technique, reliable arc initiation was obtained.

The initial experiments were performed using argon at a pressure of one atmosphere. In the first experiment an orifice diameter of 0.125 inch was used. The mass flow was 0.3 gm/sec, the power input was 16 KW and the bulk temperature was determined to be 4435°K. To obtain higher flow rates, the orifice was replaced by one of 0.188 inch diameter. During this experiment spectroscopic data were obtained. The mass flow was 0.95 gm/sec, the power input was 25 KW and the bulk temperature was

5363°K. These data are shown, together with those obtained in the small chamber and those for a vortex stabilized arc (Ref. 2), in Figure 13. At a power input of approximately 6 KW the rate of increase of bulk temperature with increasing power input for the small arc has diminished, but the increase for the large arc chamber is substantial.

The electron number density in the hot plasma core was determined by the Stark broadening of the 6032Å line in argon using the broadening data of Griem (Ref. 8). The electron number density was  $6.5 \times 10^{15}$  (cm<sup>-3</sup>). Using the equilibrium composition calculated by Drellishak et al. (Ref. 9), this corresponds to a plasma temperature of 9050°K. The plasma temperature was also determined using the ratio of the peak values of the lines 4158Å and 6032Å. The temperature determined by the line ratio method was 9133°K.

It should be noted that these temperatures are considerably higher than those obtained in the small arc (Ref. 2) where the peak arc temperature was approximately 7200°K.

The measured temperatures were compared to those predicted by theory for both the high and low frequency arcs. At a frequency of 3.5 MHz the measured temperature of 7200°K compares to a theoretical prediction of 7500°K peak temperature. At the lower frequency of 380 KHz the measured temperature of 9100°K compares to a theoretical prediction of 9300°K peak temperature. The two experiments both agree well with theory (Ref. 10), although they were performed using considerably different arc diameters and frequencies. This agreement provides further confidence that the theory can successfully be used for scaling of the electrodeless arc.

Two additional experiments were performed using argon at a pressure of two atmospheres. In the first experiment the mass flow was 1.9 gm/sec with a power input of 76 KW resulting in the highest bulk temperature recorded, 5856°K, but a heating efficiency of only 8%. In the second experiment the flow was increased to 2.4 gm/sec by reducing the power input to 63 KW. This resulted in a bulk temperature of 5300°K and increased the heating efficiency to 11%.

During the course of the experiments with argon at two atmospheres it was observed that coupling to the plasma decreased as the pressure was increased. This was evidenced by a drop in input power and a change in phase of the circuit coincident with a narrowing of the visible plasma column. A loss of coupling would be expected under these circumstances since the mutual inductance of the plasma and its driving coil will decrease as the plasma diameter decreases. This same problem became even more severe when attempts were made to operate the arc with air as the working fluid.

Numerous attempts were made to operate the arc using air as the working fluid. Many different circuit configurations were attempted in order to obtain satisfactory coupling. These included several variations of link coupling together with remote tuning of the circuit by changing the coil dimensions and, finally, an attempt was made to

operate the arc directly in the tank circuit of the oscillator. None of these techniques were successful in allowing operation with significant flow rates at pressures exceeding  $2/3$  atmosphere.

In all cases it was observed that as the flow rate and pressure were increased, the plasma diameter decreased resulting in reduced coupling and eventual extinction of the arc.

## SECTION VI

## OPERATION OF ELECTRODELESS ARCS IN AIR

Electrodeless arcs have long been successfully operated using argon as the working gas. However, few experiments have been performed using nitrogen or air and these were operated in the frequency range of several megahertz (Ref. 11).

The two primary factors which determine the behavior of the arc are the electrical conductivity and the specific heat of the gas. For a given frequency and applied magnetic field the power input depends on the radius to skin depth ratio (Ref. 12). The power input is a maximum for a value of approximately 2. For values greater than this the power input decreases. The radius to skin depth ratio is given by

$$\frac{a}{\delta} = a \sqrt{\frac{\mu}{2}} \sqrt{\sigma \omega} \quad (17)$$

where  $a$  is the radius of a cylinder of uniform conductivity  $\sigma$  in an applied field of radian frequency  $\omega$ , and  $\mu$  is the permeability of free space. To maintain an effective input of power as the frequency is decreased, it is necessary to increase the electrical conductivity. The electrical conductivity of argon and air as a function of temperature for a pressure of one atmosphere is shown in Figure 14. For the argon arc operating at 377 KHz the temperature was determined to be approximately 9000°K. This corresponds to an electrical conductivity of 24 mho/cm. For air at the same pressure the temperature required to obtain the same electrical conductivity is approximately 9900°K. At these temperatures, for equal mass flow rates, air requires approximately ten times greater power input than argon. In our system, this would have required a power input near the maximum available. To obtain this level of power input, the coupling between the generator and the load would have to be near optimum.

The degree of coupling between the plasma and the driving coil is a strong function of the ratio of coil radius to plasma radius and decreases as the plasma column decreases in diameter. The narrowing of the plasma column was observed when using air and, at higher pressures, with argon. A possible mechanism for the narrowing may be seen by referring to Figure 15, which compares the thermal conductivity for argon and air. Outside the region of the electrically conducting core, the temperature profile is largely determined by thermal conduction. In the cooler outer regions the heat flux per unit length

$$Q = 2\pi r \lambda \frac{dT}{dr}, \quad (18)$$

is approximately constant, For air in the temperature range near 7000<sup>o</sup>K, the large increase in thermal conductivity will be accompanied by a sharp decrease in the temperature gradient. This could lead to a temperature profile, shown schematically in Figure 16, which has the effect of narrowing the high temperature region of the arc, with a corresponding decrease in coupling. The loss in coupling associated with the decrease in plasma diameter, together with the requirement for greater power input combine to produce rather stringent requirements for the operation of an electrodeless arc in air.

## SECTION VII

## SUMMARY

Measurements of bulk temperatures produced by a bluff-body stabilized, atmospheric pressure arc in argon at a frequency of 3.5 MHz have been extended to higher powers and mass flow rates. The stabilizing effect of the bluff body continues to be observed at the highest mass flow rates possible with this apparatus, approximately 1 gm/sec. Measurements made at 2/3, 1 and 1-1/3 atmospheres indicate an increase in heating efficiency as the pressure is increased, although the bulk temperature was primarily a function only of power input.

Operation of an arc of similar size at a frequency of 377 KHz produced still higher bulk temperature and plasma temperature consistent with the requirement for greater electrical conductivity associated with a reduction in operating frequency. Measurements of the plasma temperature at both frequencies agree well with temperature predictions based on theory.

Attempts to operate an electrodeless arc using air at a frequency of 377 KHz at pressures of one atmosphere and greater were unsuccessful. A narrowing of the plasma column was observed, together with a decrease in coupling from the generator to the plasma. A possible explanation of the narrowing of the plasma column was based on the sharp increase in the thermal conductivity of air at temperatures near 7000°K associated with the dissociation of molecular species.

Further experiments designed to operate the electrodeless arc in air should pay particular attention to the problem of providing adequate coupling between the driving coil and the plasma. Generally, this will require that the diameter of the arc plasma be small enough to provide efficient power absorption, and that the driving coil be of no greater diameter than that required by structural considerations.

## REFERENCES

1. Reed, T. B., "The Induction Coupled Plasma Torch." J. Appl. Phys., Vol. 32, 821-824, 1961.
2. Keefer, D. R., "An Experimental Study of Electrodeless Arc Discharges." AEDC-TR-71-180, September, 1971.
3. Martin, R. E. and Keefer, D. R., "Stability Criterion for the Bluff-Body Stabilized Electrodeless Arc." Phys. Fluids, 15, 1028-1034, 1972.
4. Peters, C. E., "Ducted Turbulent Mixing Flows." Unpublished short course notes, University of Tennessee Space Institute, 1971.
5. Harloff, G. J., "Analytical Flowfield Description of the Bluff-Body Stabilized Electrodeless Arc." Master's Thesis, University of Florida, 1972.
6. Stoever, H. J., Applied Heat Transmission, McGraw-Hill, New York, 1941.
7. Roark, R. J., Formulas for Stress and Strain, McGraw-Hill, New York, 1954.
8. Griem, H., Plasma Spectroscopy, McGraw-Hill, New York, 1964.
9. Drellishak, K. S., Knopp, C. F., and Cambel, A. B., "Partition Functions and Thermodynamic Properties of Argon Plasma." AEDC-TDR-63-146, August, 1963.
10. Keefer, D. R., Sprouse, J. A., and Loper, F. C., "The Confined Electrodeless Arc." Bulletin of the American Physical Society, Ser. II, Vol. 15, No. 3, pp. 413, March, 1970.
11. Eckert, H. U., Kelly, F. L., and Olsen, H. N., "Spectroscopic Observations on Induction-Coupled Plasma Flames in Air and Argon." J. Appl. Phys. 39, 1846-1852, 1968.
12. Henriksen, B. B., Keefer, D. R., and Clarkson, M. H., "Electromagnetic Field in Electrodeless Discharge." J. Appl. Phys., 42, 5460-5464, 1971.

TABLE 1  
 Small Arc Chamber Data,  
 .125 and .1875 Reamed Orifices

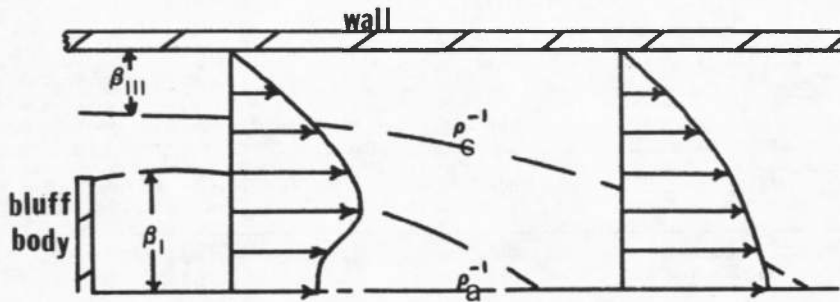
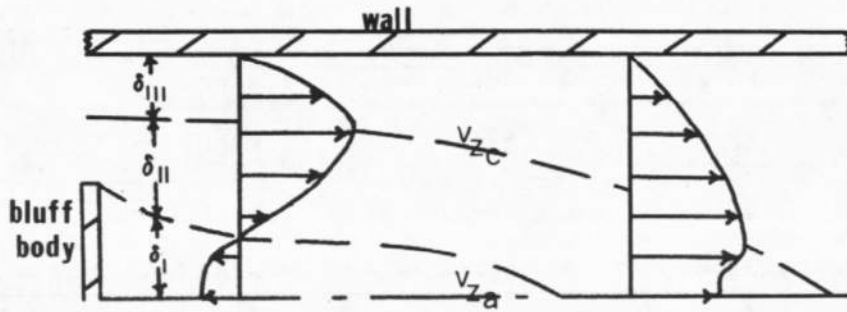
Orifice Diameter (inches)	Mass Flow Rate (gm/sec)	Input Power (kw)	Bulk Gas Temperature ( $^{\circ}$ K)	Enthalpy (cal/gm)	Efficiency (%)
.125	.598	6.01	2517	312.1	13.0
.125	.624	4.14	2374	294.4	18.6
.125	.701	3.68	2016	250.0	19.9
.1875	.992	5.54	2248	278.8	20.9
.1875	1.026	6.79	2305	285.8	18.1

TABLE 2  
 Small Arc Chamber Data,  
 128 Laval Shaped Orifice

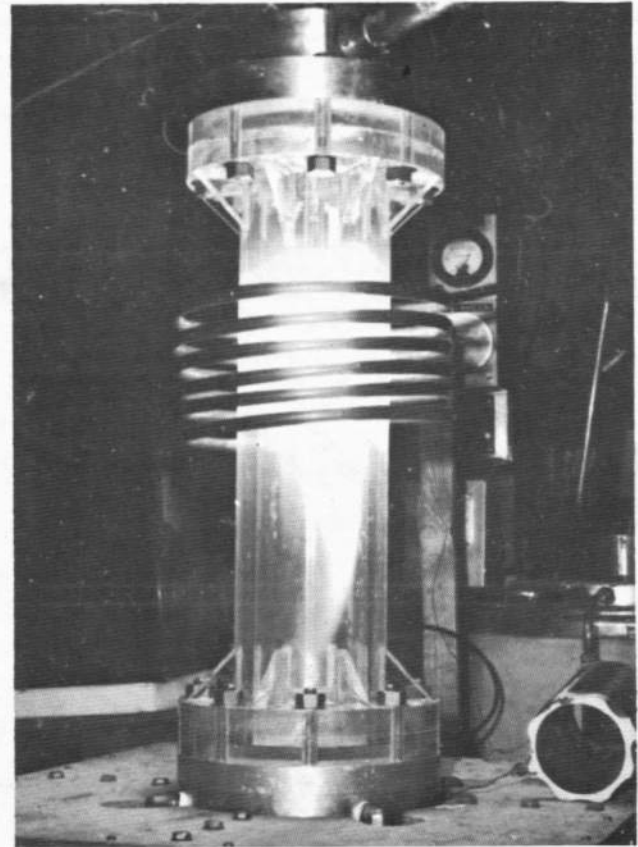
Chamber Pressure (inHg)	Mass Flow Rate (gm/sec)	Input Power (kw)	Bulk Gas Temperature (°K)	Enthalpy (cal/gm)	Heating Efficiency (%)
19.8	.419	5.81	3962	491.3	14.8
19.8	.419	5.38	3962	491.3	16.0
19.8	.428	4.79	3797	470.8	17.6
19.8	.428	4.49	3797	470.8	18.9
19.8	.428	4.32	3797	470.8	19.5
19.8	.436	3.50	3675	455.7	23.7
29.6	.606	6.23	4233	524.9	21.4
29.6	.615	6.38	4110	509.6	20.6
29.6	.615	5.28	4110	509.6	24.9
29.6	.624	5.74	3992	495.0	22.5
29.6	.633	4.86	3879	481.0	26.2
29.6	.633	4.48	3879	481.0	28.4

TABLE 2 - Continued

Chamber Pressure (inhg)	Mass Flow Rate (gm/sec)	Input Power (kw)	Bulk Gas Temperature ( <sup>o</sup> K)	Enthalpy (cal/gm)	Heating Efficiency (%)
29.6	.633	4.42	3879	481.0	28.8
29.6	.641	4.36	3783	469.1	28.9
29.6	.650	4.10	3679	456.2	30.3
29.6	.658	4.10	3590	445.2	29.9
39.8	.813	7.25	4252	527.2	24.7
39.8	.822	6.32	4159	515.7	28.0
39.8	.829	6.39	4089	507.0	27.5
39.8	.829	6.11	4089	507.0	28.8
39.8	.855	5.76	3844	476.7	29.6
39.8	.855	5.42	3844	476.7	31.5
39.8	.872	5.22	3696	458.3	32.0
39.8	.906	4.68	3423	424.4	34.4



(a)



(b)

Fig. 1 Model for boundary layer analysis showing velocity boundary layers,  $\delta$ , and thermal boundary layers  $\beta$ .

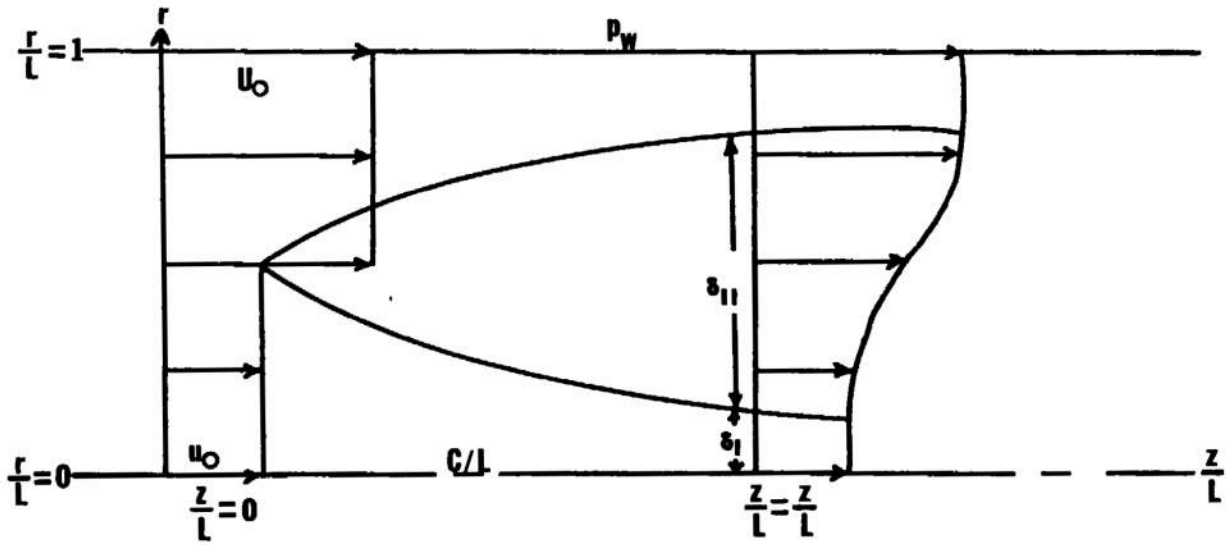


Fig. 2 Simplified Boundary Layer model for incompressible flow without heat addition .

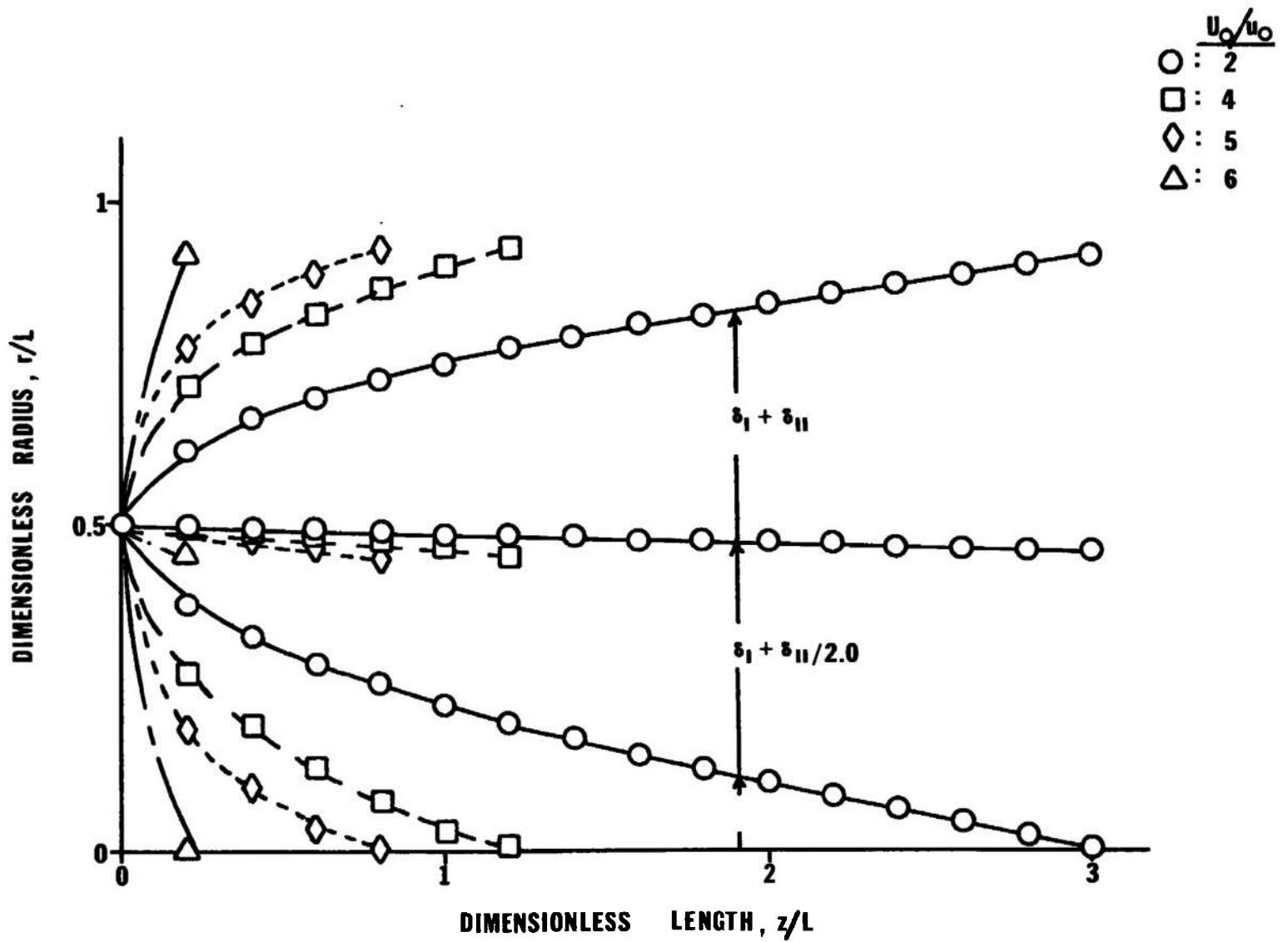


Fig. 3 Calculated boundary layer profiles for a Reynolds number of 300 .

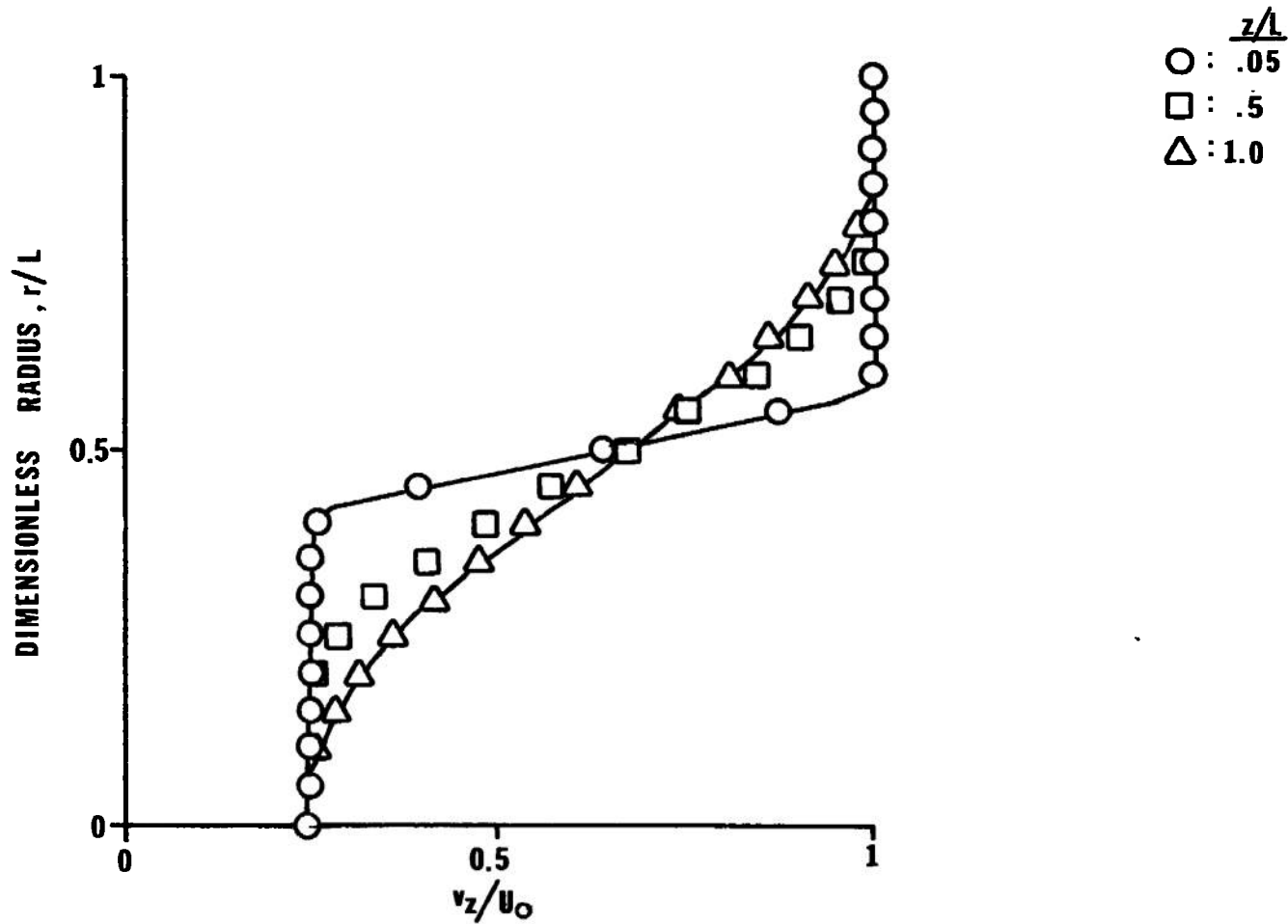


Fig. 4 Axial velocity profiles at three axial locations. Reynolds number = 300,  $U_0/u_0 = 4$ .

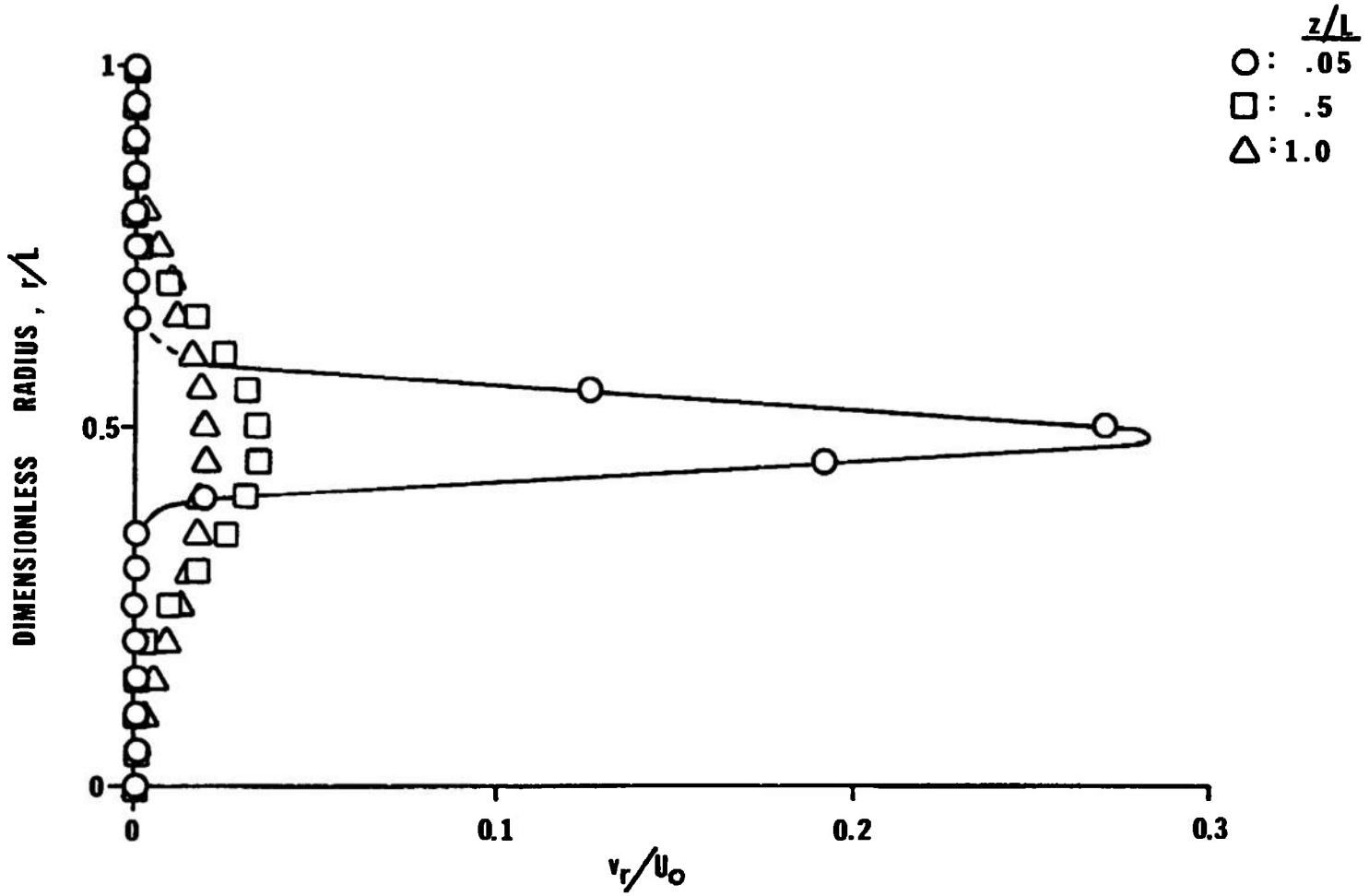


Fig. 5 Radial velocity profiles at three axial locations. Reynolds number = 300,  $U_0/u_0 = 4$ .

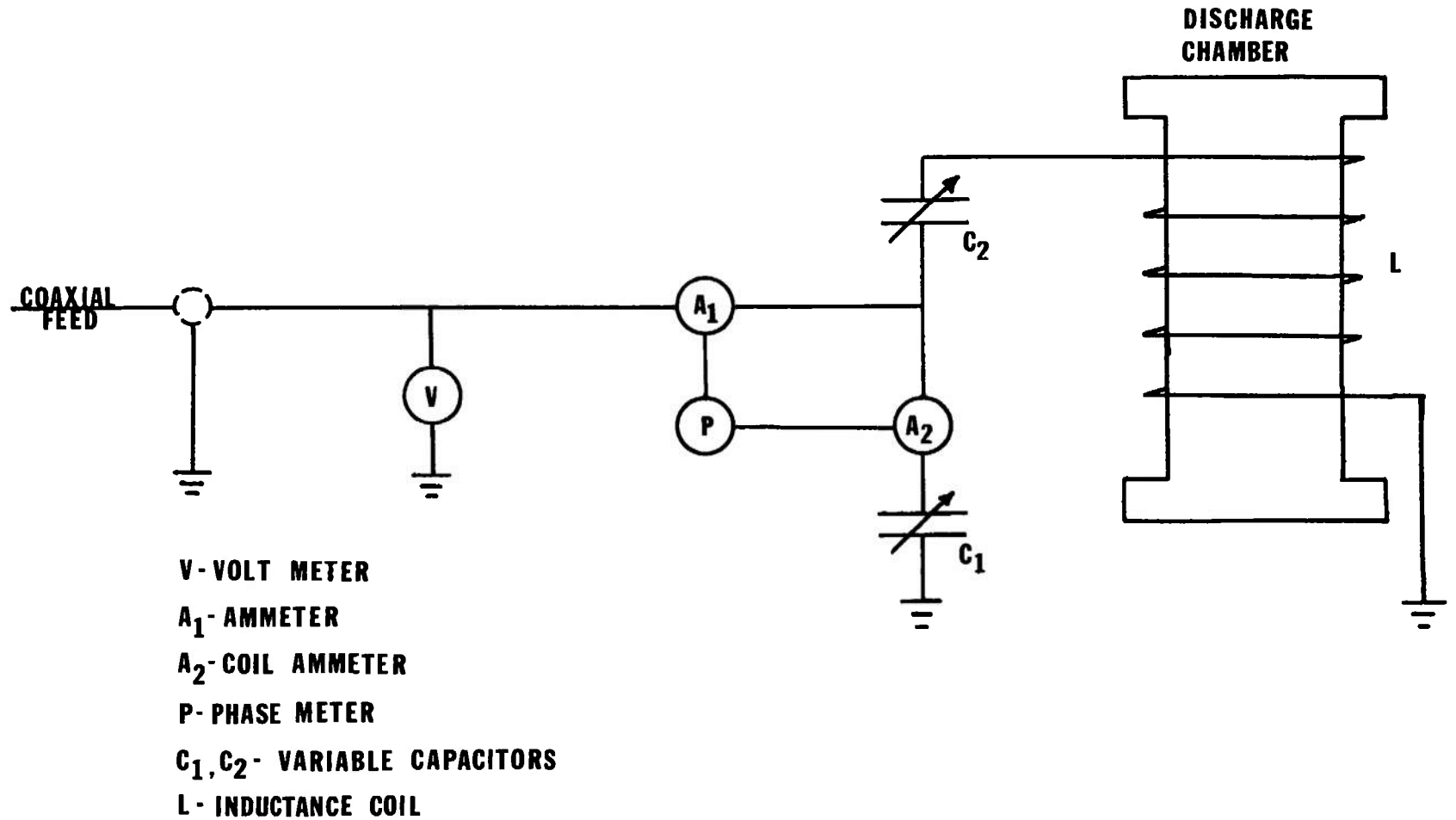


Fig. 6 Remote tuned circuit used in the 4.5 MHz experiments .

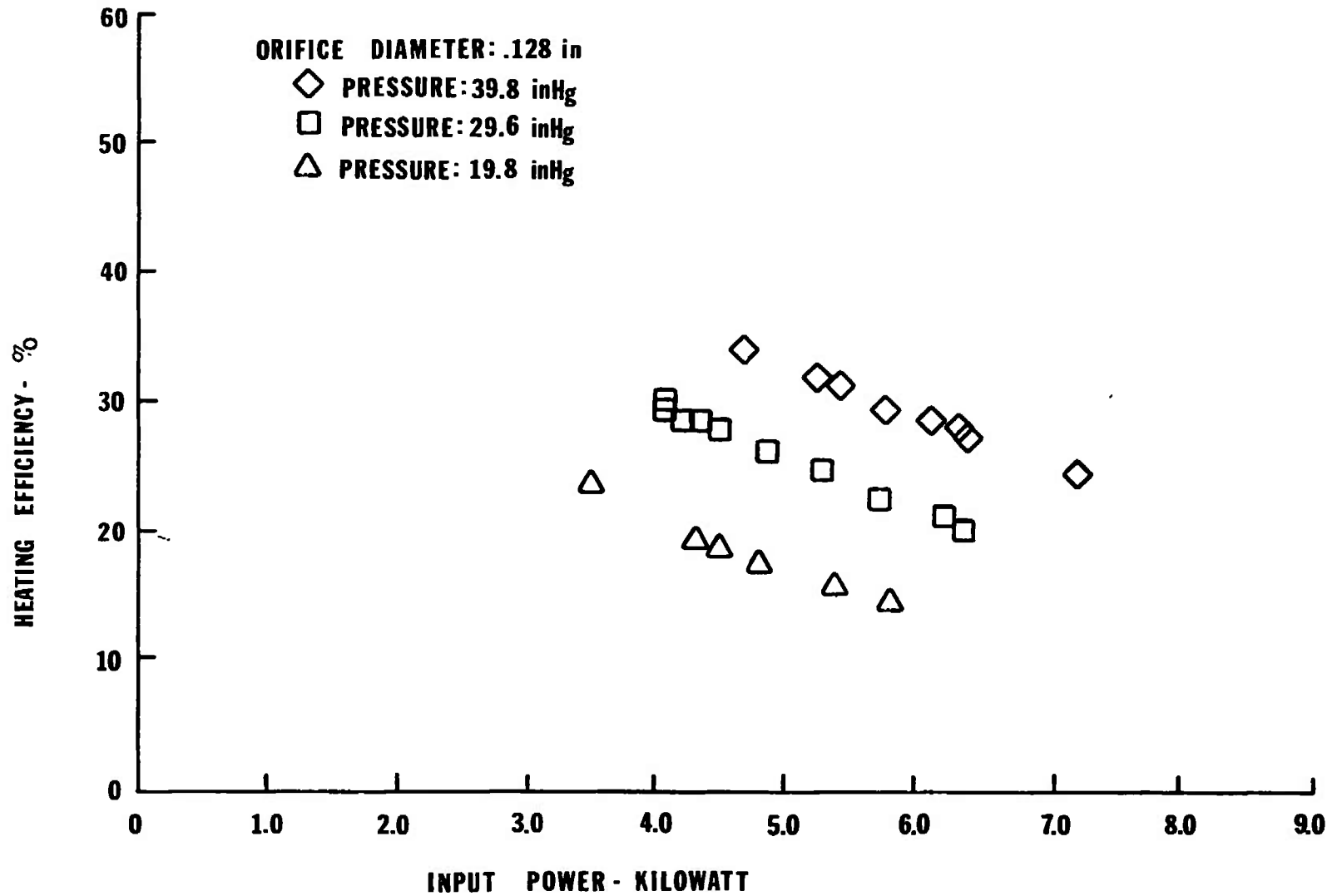


Fig. 7 Heating efficiency of the 4.5 MHz arc at three values of pressure.

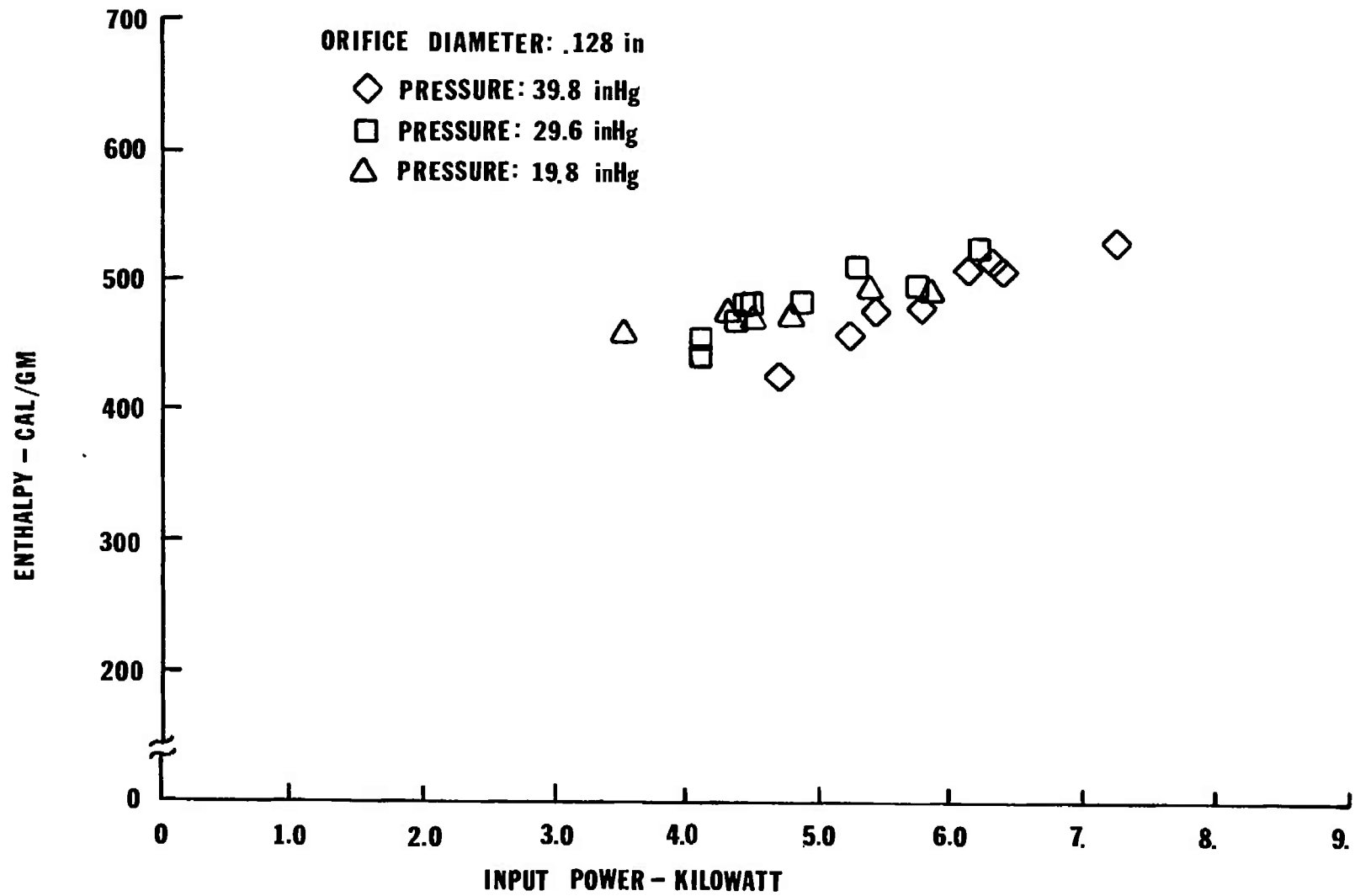


Fig. 8 Enthalpy for the 4.5 MHz arc at three values of pressure.

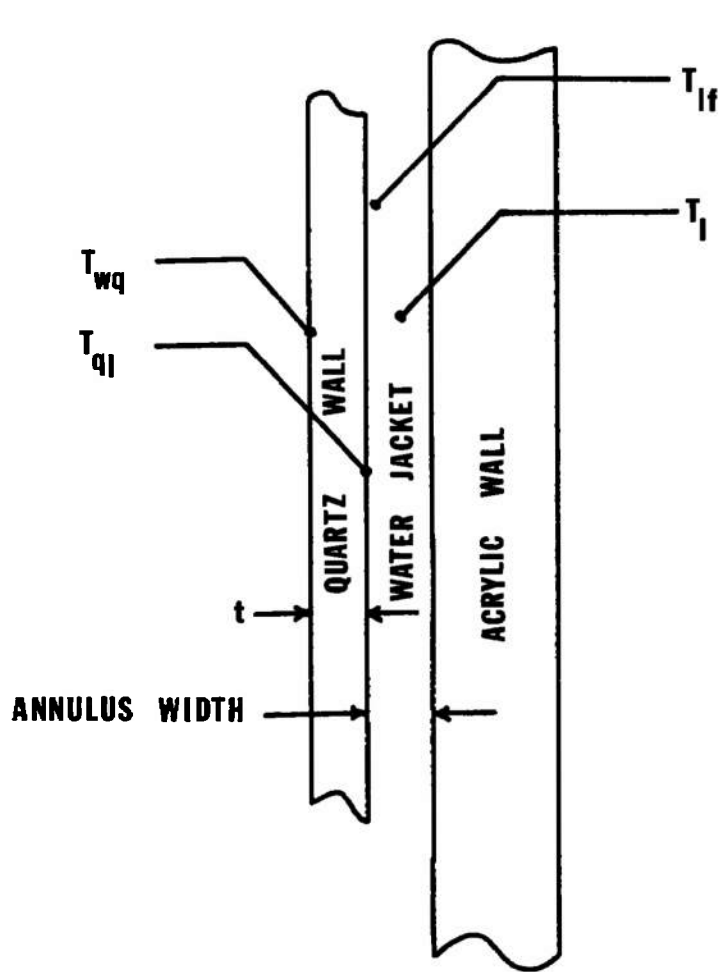


Fig. 9 Temperatures used in the design analysis .

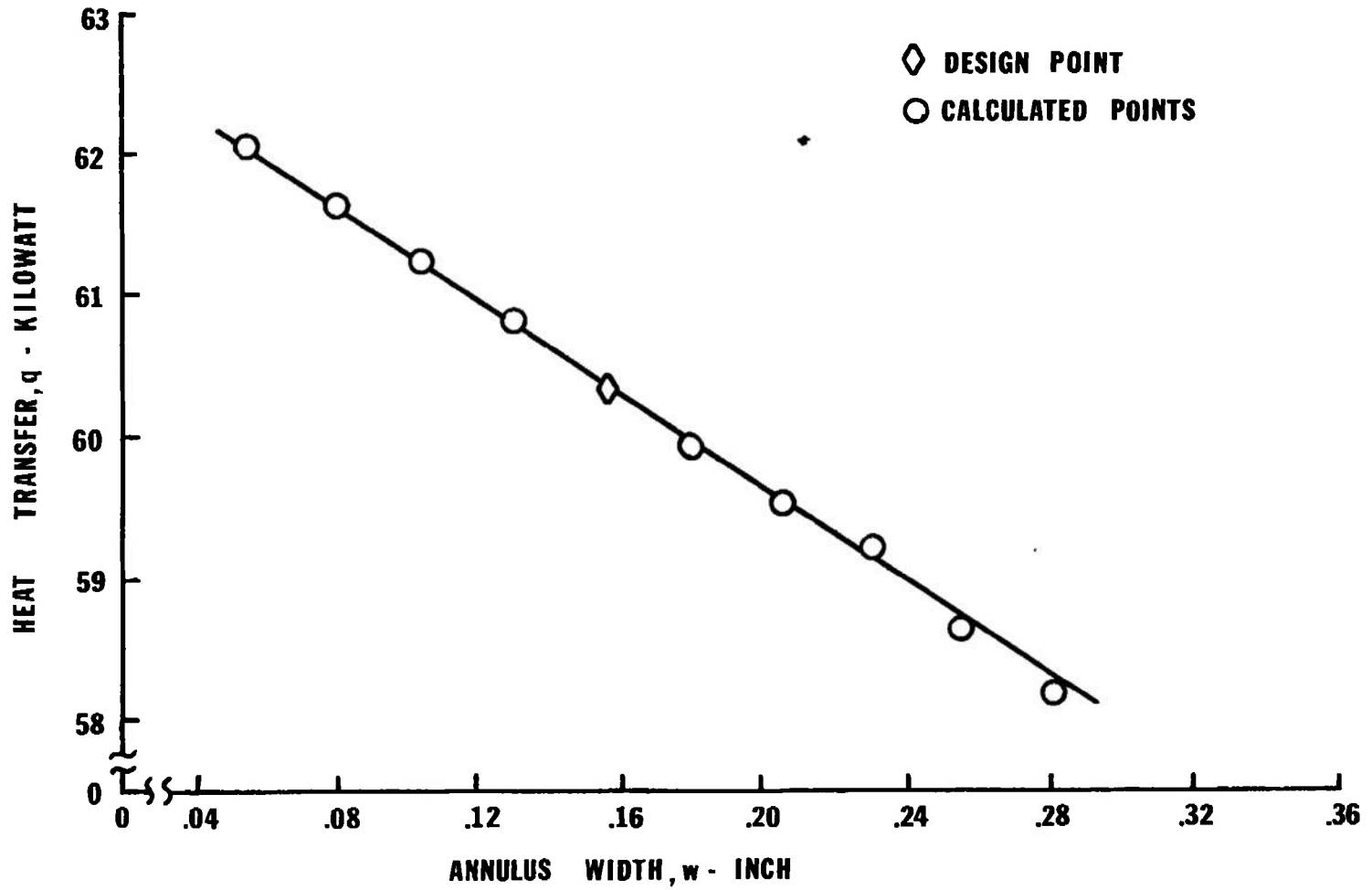


Fig. 10 Heat transfer rate as a function of annulus width .

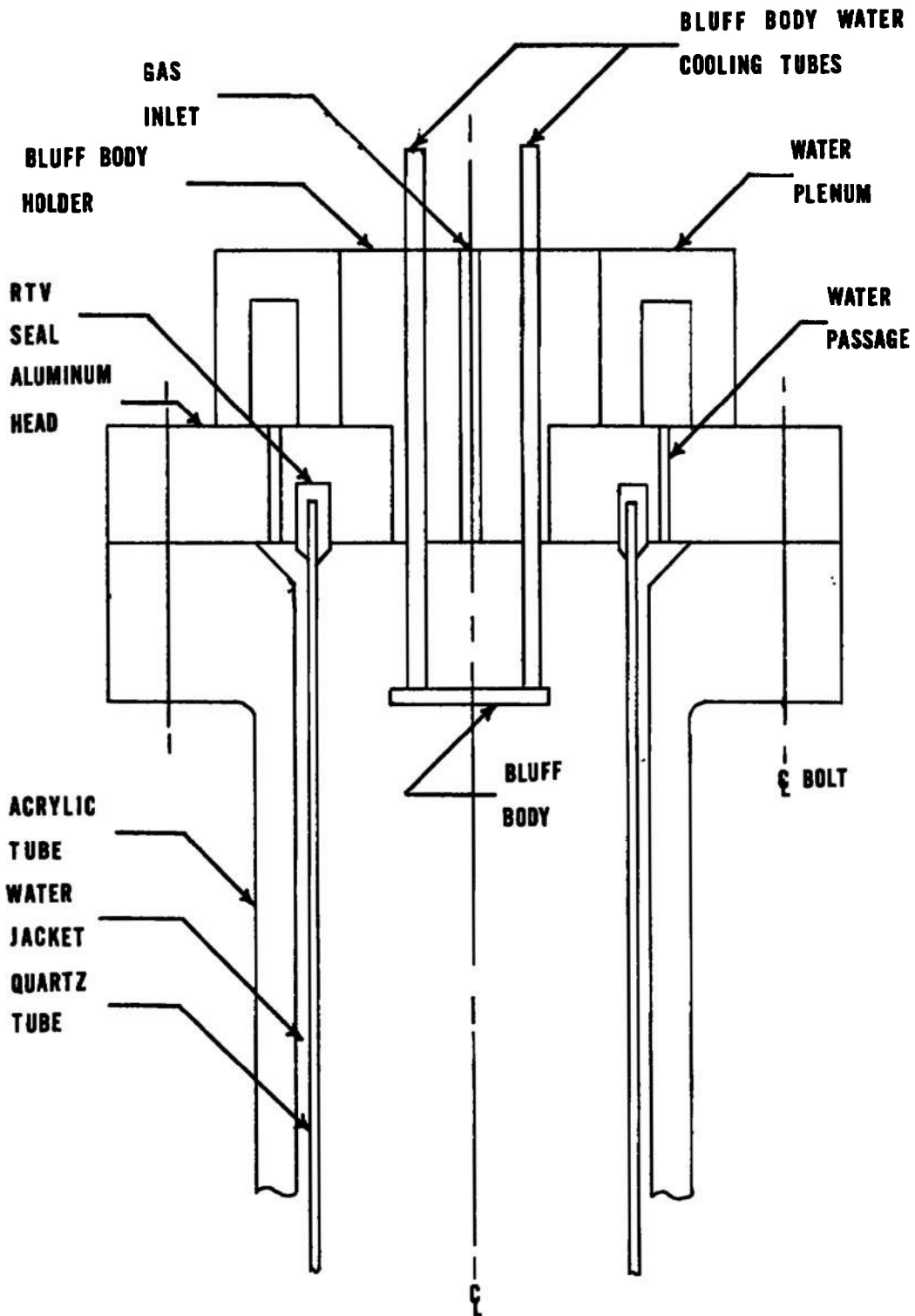


Fig. 11 Upper portion of the large arc chamber .

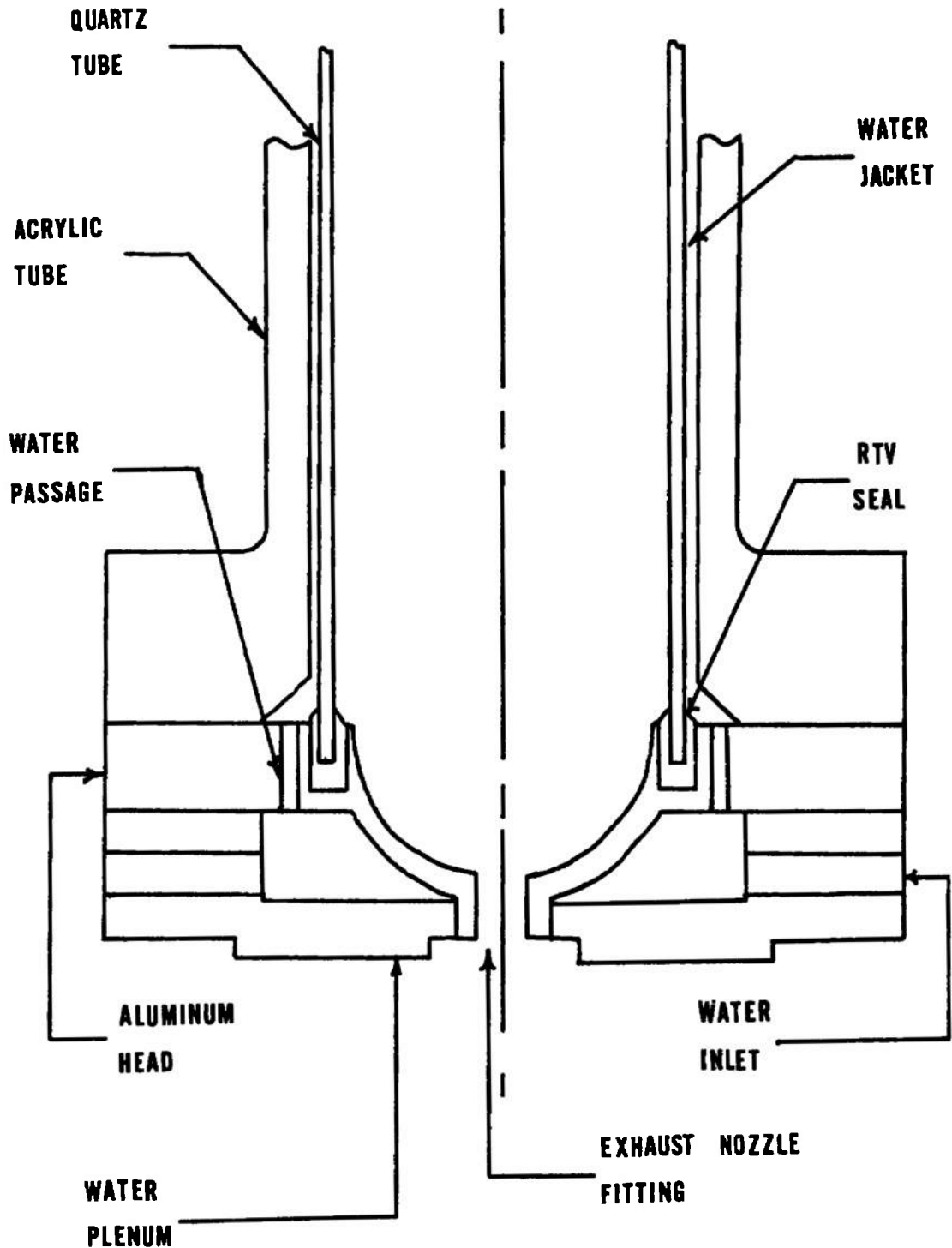


Fig. 12 Lower portion of the large arc chamber .

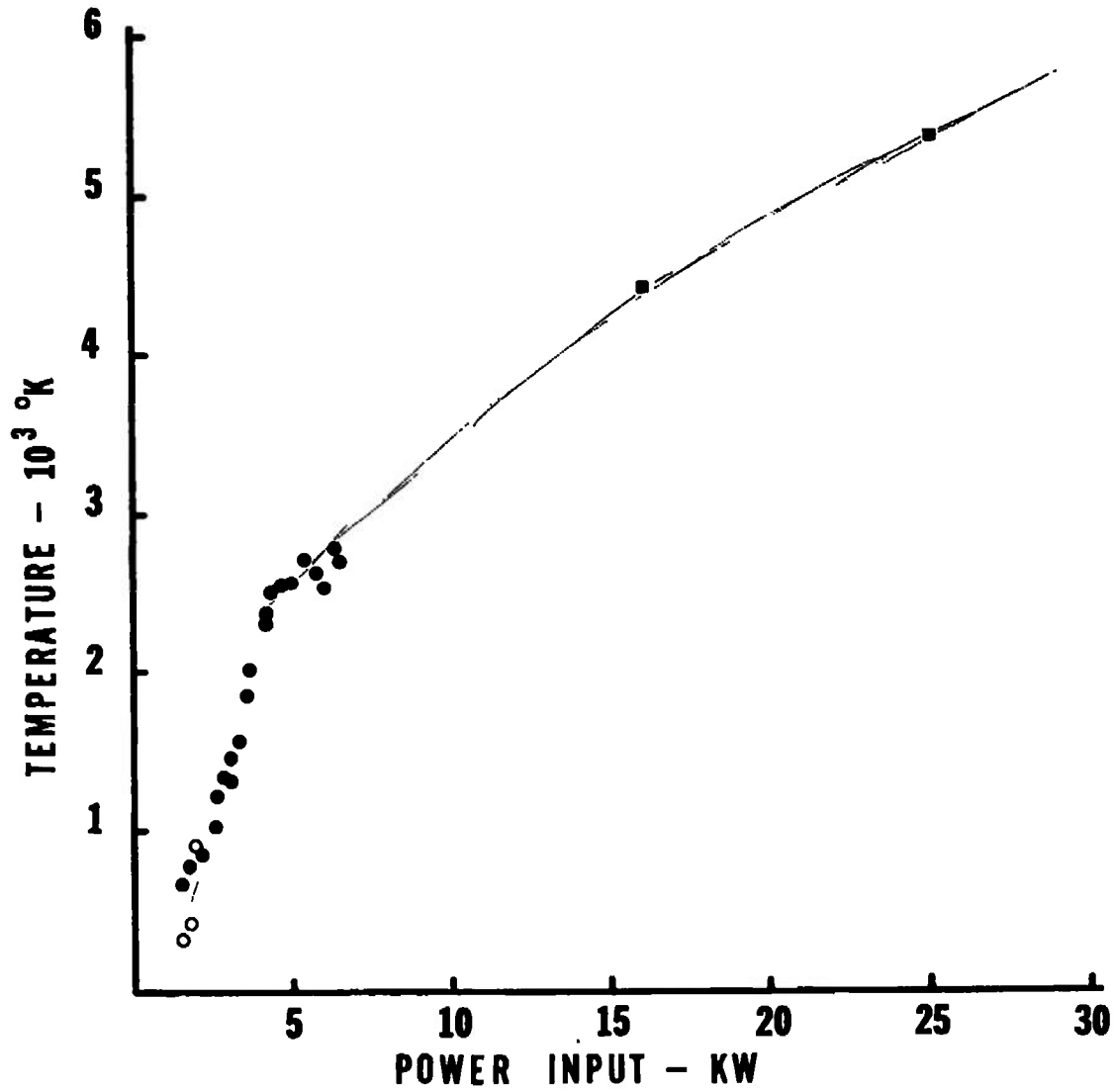


Fig. 13 Bulk temperatures in 3 electrodeless arcs. Open circles are for 4.5 MHz vortex stabilized arc, closed circles are for 4.5 MHz bluff-body stabilized arc and squares are for 3.77 MHz bluff-body stabilized arc.

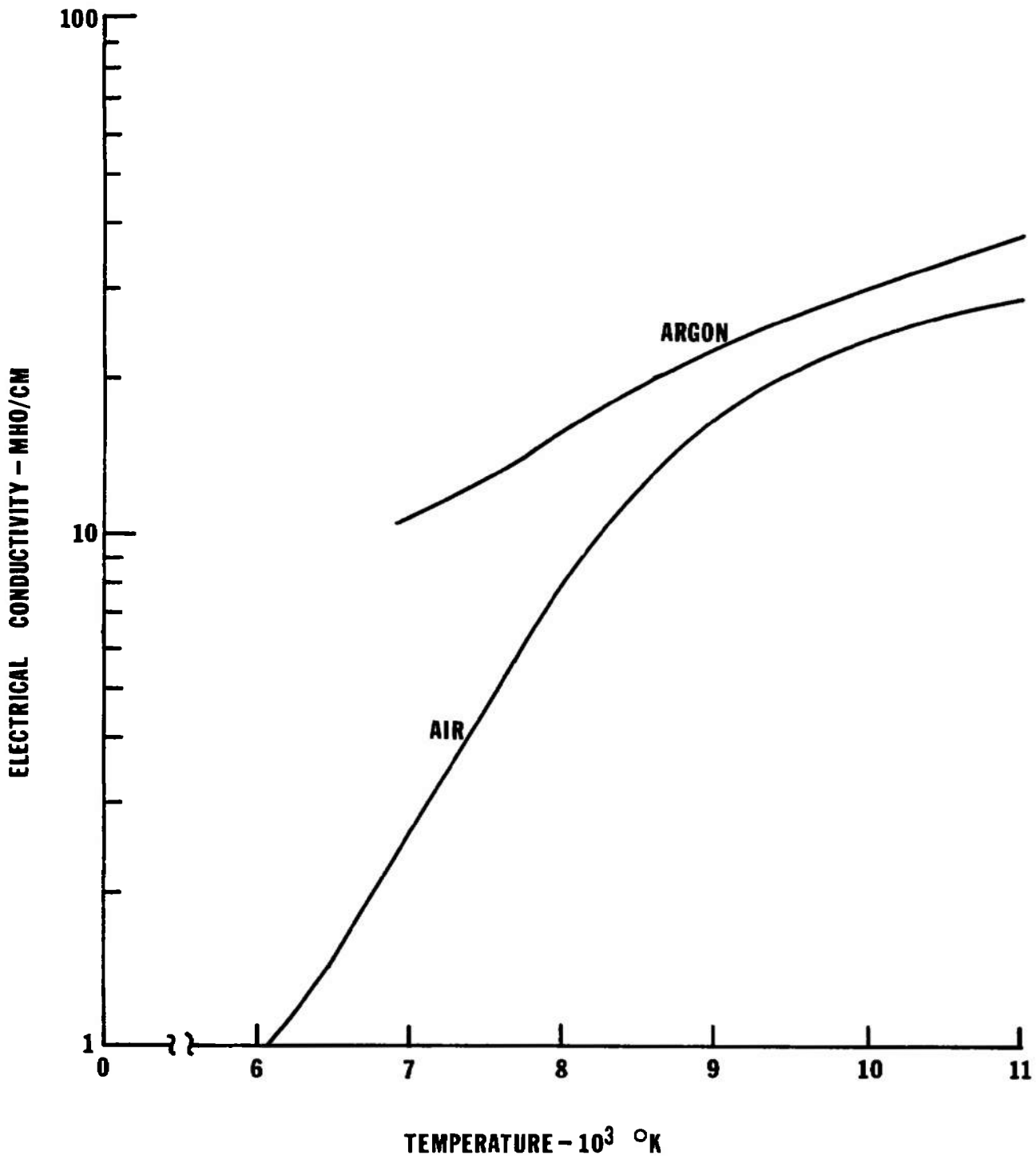


Fig. 14 Electrical conductivity of argon and air at one atmosphere .

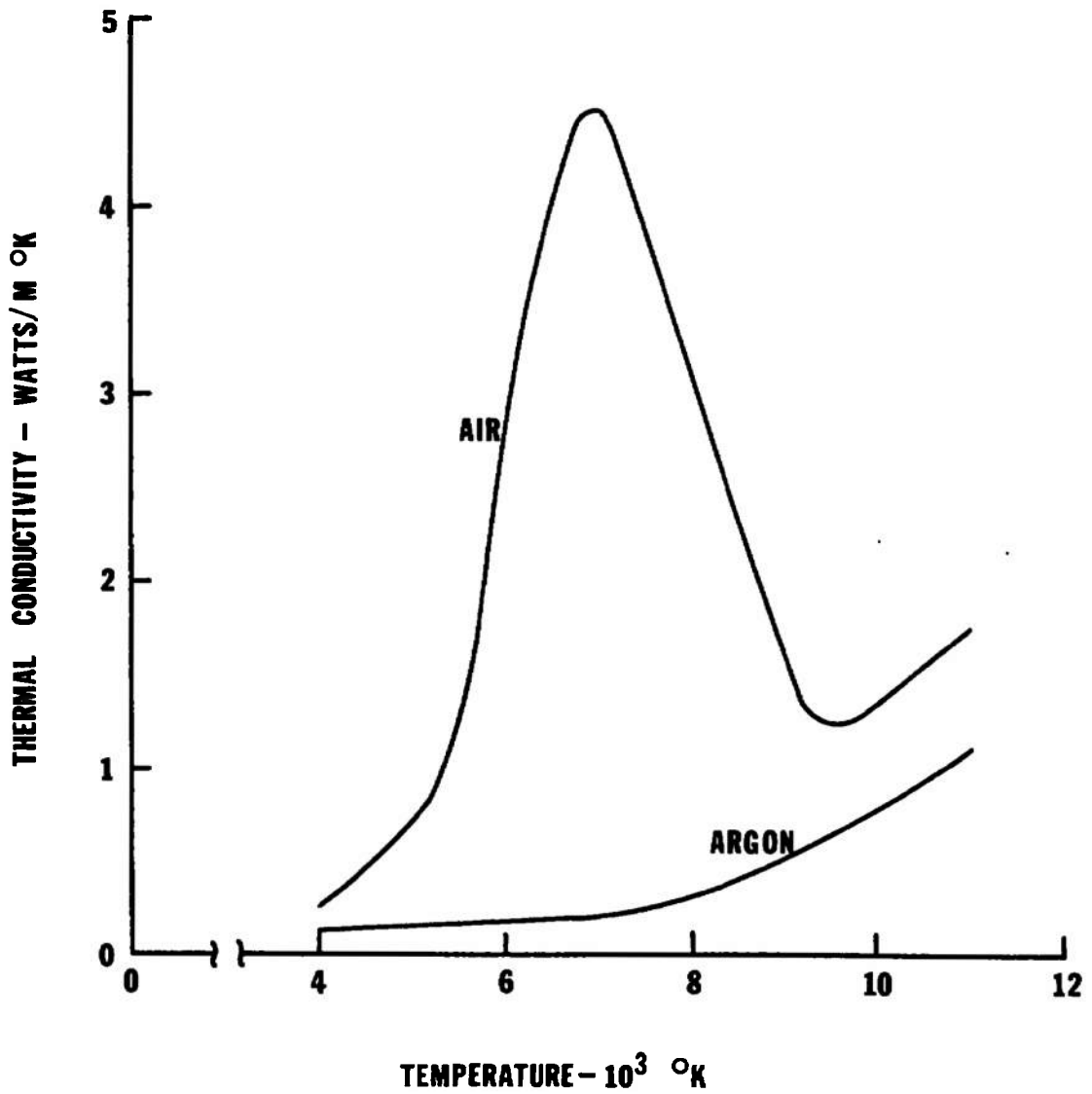


Fig. 15 Thermal conductivity of argon and air at one atmosphere .

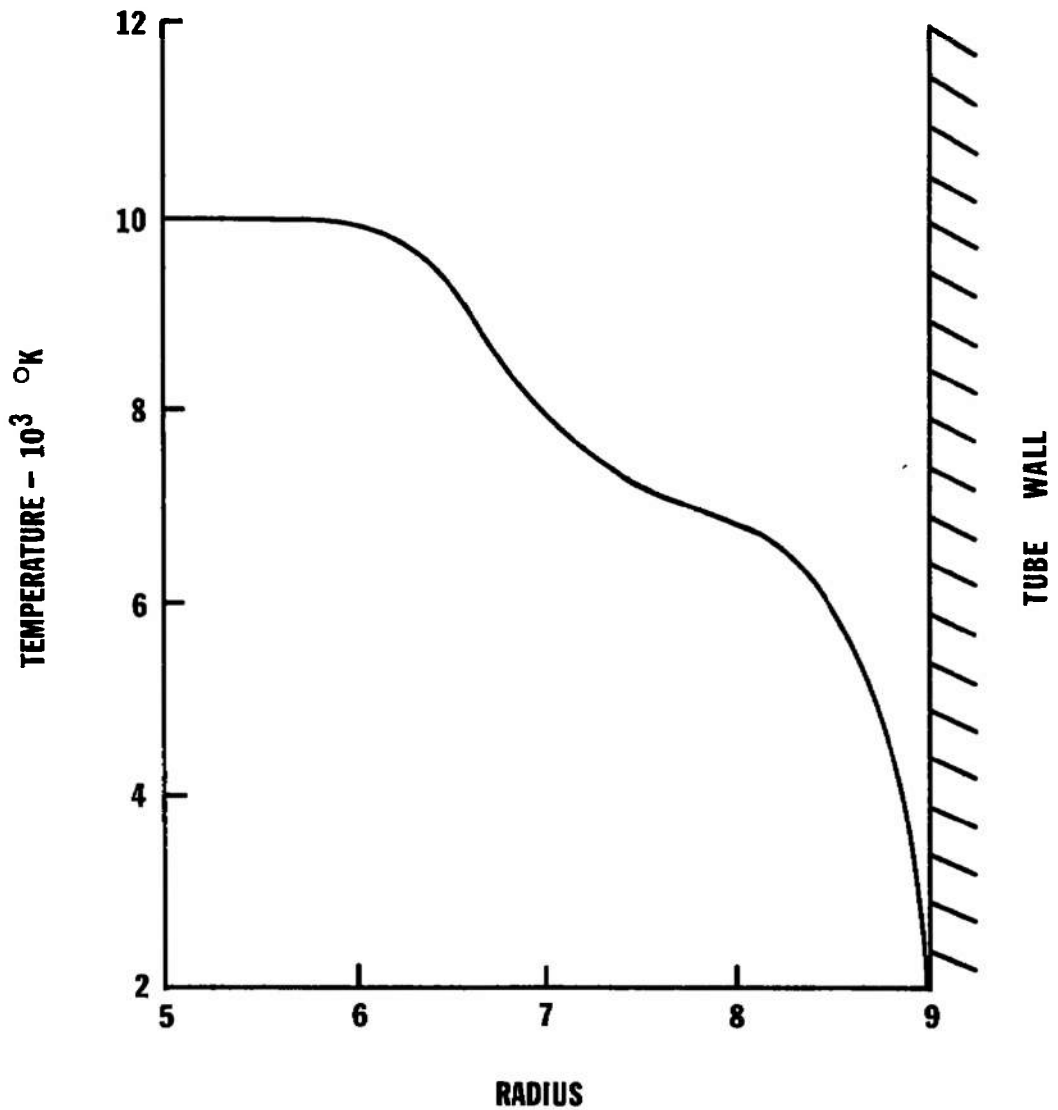


Fig. 16 Possible temperature profile resulting from increase in thermal conductivity associated with molecular dissociation of air.

UNCLASSIFIED

Security Classification

DOCUMENT CONTROL DATA - R & D

(Security classification of title, body of abstract and indexing annotation must be entered when the overall report is classified)

1 ORIGINATING ACTIVITY (Corporate author) University of Florida Gainesville, Florida 32601		2a. REPORT SECURITY CLASSIFICATION UNCLASSIFIED	
		2b. GROUP N/A	
3 REPORT TITLE A STUDY OF ELECTRODELESS ARC DISCHARGE USING ARGON, NITROGEN, AND AIR			
4 DESCRIPTIVE NOTES (Type of report and Inclusive dates) Final Report -- January 1972 to March 1973			
5 AUTHOR(S) (First name, middle initial, last name) Dennis R. Keefer			
6 REPORT DATE September 1973	7a. TOTAL NO OF PAGES 45	7b. NO OF REFS 12	
8a. CONTRACT OR GRANT NO F40600-72-C-0005	9a. ORIGINATOR'S REPORT NUMBER(S) AEDC-TR-73-143		
b. PROJECT NO	9b. OTHER REPORT NO(S) (Any other numbers that may be assigned this report)		
c. Program Element 65802F			
d			
10. DISTRIBUTION STATEMENT Approved for public release; distribution unlimited.			
11 SUPPLEMENTARY NOTES Available in DDC.		12 SPONSORING MILITARY ACTIVITY Arnold Engineering Development Center, Air Force Systems Command, Arnold AF Station, TN 37389	
13 ABSTRACT A study of the bluff-body stabilized electrodeless arc was undertaken to extend the operation to greater mass flow rates and power input. A small arc chamber, operating at a frequency of 3.5 MHz, was operated with mass flows up to 1.026 gm/sec of argon at atmospheric pressure with a power input of 6.79 KW. Under these conditions a plasma bulk temperature of 2305°K was obtained with a heating efficiency of 18%. It was found that heating efficiency increased with chamber pressure, but bulk temperature depends primarily upon the power input. A larger arc chamber was designed for a nominal power input of 200 KW at a frequency of 377 MHz. This chamber was operated at mass flow rates up to 2.4 gm/sec of argon at a pressure of two atmospheres. A plasma bulk temperature of 5856°K was obtained at a power input of 76 KW. Attempted operation using air as a working fluid was unsuccessful at pressures in excess of 2/3 atmosphere due to inefficient coupling to the arc plasma.			

UNCLASSIFIED

Security Classification

14. KEY WORDS	LINK A		LINK B		LINK C	
	ROLE	WT	ROLE	WT	ROLE	WT
electric arcs electric discharges temperature measurements plasma diagnostics argon nitrogen air						

AFSC  
Arnold AFB Tex

UNCLASSIFIED

Security Classification